



THE UNIVERSITY *of* EDINBURGH

## Edinburgh Research Explorer

### High-pressure Raman studies and heat capacity measurements on the MgSiO<sub>3</sub> analogue Calr<sub>0.5</sub>Pt<sub>0.5</sub>O<sub>3</sub>

**Citation for published version:**

Hirai, S, Kojima, Y, Ohfuji, H, Nishiyama, N, Irifune, T, Klemme, S, Bromiley, G & Attfield, JP 2011, 'High-pressure Raman studies and heat capacity measurements on the MgSiO<sub>3</sub> analogue Calr<sub>0.5</sub>Pt<sub>0.5</sub>O<sub>3</sub>', *Physics and Chemistry of Minerals*, vol. 38, no. 8, pp. 631-637. <https://doi.org/10.1007/s00269-011-0435-2>

**Digital Object Identifier (DOI):**

[10.1007/s00269-011-0435-2](https://doi.org/10.1007/s00269-011-0435-2)

**Link:**

[Link to publication record in Edinburgh Research Explorer](#)

**Document Version:**

Peer reviewed version

**Published In:**

Physics and Chemistry of Minerals

**Publisher Rights Statement:**

Final publication copyright of Springer-Verlag (2011) available at <http://link.springer.com/article/10.1007%2Fs00269-011-0435-2>

**General rights**

Copyright for the publications made accessible via the Edinburgh Research Explorer is retained by the author(s) and / or other copyright owners and it is a condition of accessing these publications that users recognise and abide by the legal requirements associated with these rights.

**Take down policy**

The University of Edinburgh has made every reasonable effort to ensure that Edinburgh Research Explorer content complies with UK legislation. If you believe that the public display of this file breaches copyright please contact [openaccess@ed.ac.uk](mailto:openaccess@ed.ac.uk) providing details, and we will remove access to the work immediately and investigate your claim.



Cite As: Hirai, S, Kojima, Y, Ohfuji, H, Nishiyama, N, Irifune, T, Klemme, S, Bromiley, G & Attfield, JP 2011, 'High-pressure Raman studies and heat capacity measurements on the MgSiO<sub>3</sub> analogue CaIr<sub>0.5</sub>Pt<sub>0.5</sub>O<sub>3</sub>' *Physics and chemistry of minerals*, vol 38, no. 8, pp. 631-637.

DOI: 10.1007/s00269-011-0435-2

## High-pressure Raman studies on post-perovskite solid solution CaIr<sub>0.5</sub>Pt<sub>0.5</sub>O<sub>3</sub> and room-pressure Raman studies on CaIr<sub>1-x</sub>Pt<sub>x</sub>O<sub>3</sub> (x = 0, 0.3, 0.5, 0.7) & CaIr<sub>0.5</sub>Rh<sub>0.5</sub>O<sub>3</sub>

Shigeto Hirai<sup>\*</sup>, Yohei Kojima<sup>\*\*</sup>, Hiroaki Ohfuji<sup>\*\*</sup>, Norimasa Nishiyama<sup>\*\*</sup>, Tetsuo Irifune<sup>\*\*</sup>, Stephan Klemme<sup>\*\*\*</sup>, Geoffrey Bromiley<sup>\*</sup> and J. Paul Attfield<sup>\*\*\*\*</sup>

<sup>\*</sup>Centre for Science at Extreme Conditions and School of Geosciences, University of Edinburgh, Mayfield Road, Edinburgh EH9 3JZ, UK

<sup>\*\*</sup>Geodynamics Research Center, Ehime University, 2-5 Bunkyo-cho, Matsuyama, Ehime 790-8577, Japan

<sup>\*\*\*</sup>Institut für Mineralogie, Corrensstr. 24, Universität Münster, 48149 Münster, Germany

<sup>\*\*\*\*</sup>Centre for Science at Extreme Conditions and School of Chemistry, University of Edinburgh, Mayfield Road, Edinburgh EH9 3JZ, UK

**Abstract:** High-quality polycrystalline samples of CaIr<sub>1-x</sub>Pt<sub>x</sub>O<sub>3</sub> (x = 0.3, 0.5, 0.7) and CaIr<sub>0.5</sub>Rh<sub>0.5</sub>O<sub>3</sub> have been obtained at a pressure of 15 GPa, and high-pressure Raman studies on CaIr<sub>0.5</sub>Pt<sub>0.5</sub>O<sub>3</sub> and room-pressure Raman studies on CaIr<sub>1-x</sub>Pt<sub>x</sub>O<sub>3</sub> series (x = 0, 0.3, 0.5, 0.7) and CaIr<sub>0.5</sub>Rh<sub>0.5</sub>O<sub>3</sub> are reported. A new phase of CaIr<sub>0.5</sub>Pt<sub>0.5</sub>O<sub>3</sub> synthesized at 60GPa, 1900K has Raman modes which resemble those of CaIrO<sub>3</sub> perovskite, suggesting this phase has a perovskite structure. Pt-O covalent bonding stabilizes the post-perovskite structure and destabilizes the perovskite structure, whilst pressure and the replacement of Pt-O by Ir-O bonding also stabilises the perovskite structure. The instability of the perovskite phase of CaIr<sub>0.5</sub>Pt<sub>0.5</sub>O<sub>3</sub> reveals why the post-perovskite to perovskite phase transition has not been observed for CaPtO<sub>3</sub> unlike the case for CaIrO<sub>3</sub>, CaRhO<sub>3</sub> and CaRuO<sub>3</sub>.

## I. Introduction

Since the discovery of the perovskite to post-perovskite transition in  $\text{MgSiO}_3$  in a laser-heated diamond anvil cell<sup>1</sup>, wide attention has been focussed on the post-perovskite phase of  $\text{MgSiO}_3$ . This is because the post-perovskite phase is likely to play a key role in processes occurring in Earth's lower mantle, and the perovskite to post-perovskite transition can explain many features of the D'' seismic discontinuity there. While it is important to conduct further studies on  $\text{MgSiO}_3$ , this post-perovskite phase cannot be quenched to ambient conditions; this is also the case for the post-perovskite type transition metal oxides  $\text{Fe}_2\text{O}_3$ <sup>2</sup> and  $\text{Mn}_2\text{O}_3$ <sup>3</sup>. Thus, it is useful to investigate structural analogues of the  $\text{MgSiO}_3$  post-perovskite that are quenchable to ambient conditions.

The post-perovskite phase of  $\text{MgSiO}_3$  adopts the layered structure  $\text{CaIrO}_3$ -structure containing corner-linked chains of edge-sharing octahedra (Fig.1). Four quenchable  $\text{CaIrO}_3$ -type oxides have been reported to date:  $\text{CaIrO}_3$ <sup>4</sup>,  $\text{CaPtO}_3$ <sup>5</sup>,  $\text{CaRhO}_3$ <sup>6</sup> and  $\text{CaRuO}_3$ <sup>7</sup>. Polycrystalline  $\text{CaIrO}_3$  can be synthesized at ambient pressure from binary oxides heated to 1273 K in an evacuated silica tube, and single crystals of  $\text{CaIrO}_3$  were synthesized at 1223 K using a  $\text{CaCl}_2$  flux.<sup>4</sup> The other three oxides were obtained using a multi-anvil apparatus to achieve high pressure-temperature conditions;  $\text{CaPtO}_3$  (4GPa, 1073K),<sup>5</sup>  $\text{CaRhO}_3$  (6GPa, 1473K)<sup>6</sup> and  $\text{CaRuO}_3$  (23GPa, 1223K).<sup>7</sup> need high pressure/temperature condition for synthesis. Further studies on these materials have revealed post-perovskite to perovskite structural phase transitions at high P-T. The post-perovskite phase of  $\text{CaIrO}_3$  transforms to the perovskite structure at 2GPa, 1673K<sup>8</sup> and this transformation was also observed for  $\text{CaRhO}_3$  (6GPa, 1873K) and  $\text{CaRuO}_3$  (23GPa, 1343K), while  $\text{CaPtO}_3$  remained post-perovskite at higher temperatures<sup>9</sup>. The former observations show that the perovskite type is the high temperature phase and this was supported by a Raman spectroscopy study of  $\text{CaIrO}_3$  up to 30GPa<sup>10</sup> and a synchrotron X-ray diffraction of  $\text{CaPtO}_3$  up to 40GPa<sup>11</sup> which show that the phase transition from post-perovskite to perovskite transition does not occur at room temperature.

The presence of heavy transition metal ions in the above  $\text{CaMO}_3$  post-perovskites suggests that such phases might have interesting electronic or magnetic properties. A study of  $\text{Ca}_{1-x}\text{Na}_x\text{IrO}_3$  solid solutions (synthesized at 4GPa, 1073K)<sup>12</sup> revealed a metal-insulator transition at  $x = 0.37$ . To investigate such properties further, we have explored the  $\text{CaIr}_{1-x}\text{Pt}_x\text{O}_3$  series and the synthesis, structural and physical properties of these solid solutions are reported here. We

have also demonstrated that  $\text{CaIr}_{1-x}\text{Rh}_x\text{O}_3$  materials are accessible and we report the  $x = 0.5$  member of this series.

## II. Experimental Section

Polycrystalline samples of  $\text{CaIrO}_3$  post-perovskite were synthesized by solid state reaction from  $\text{CaO}$  and  $\text{IrO}_2$ .  $\text{CaO}$  powder was prepared from  $\text{CaCO}_3$  by heating in air at  $1000^\circ\text{C}$  for 24 hrs. Well-ground mixtures of the starting material in a stoichiometric molar ratio were sealed in an evacuated silica tube, and heated in air at  $1273\text{K}$  over 20 hrs.  $\text{CaIrO}_3$  post-perovskite single crystals were synthesized by flux method<sup>4</sup>. Polycrystalline samples of the perovskite phase of  $\text{CaIrO}_3$  were synthesized by solid state reaction from  $\text{CaO}$  and  $\text{IrO}_2$ . Well-ground mixtures of the starting material in a stoichiometric molar ratio were sealed in an evacuated silica tube, and heated in air at  $930^\circ\text{C}$  over 60 hrs.

Polycrystalline samples of  $\text{CaIr}_{1-x}\text{Pt}_x\text{O}_3$  and  $\text{CaIr}_{0.5}\text{Rh}_{0.5}\text{O}_3$  were synthesized at high pressure-temperature conditions.  $\text{CaIr}_{1-x}\text{Pt}_x\text{O}_3$  ( $x = 0.3, 0.5, 0.7$ ) were synthesized by solid-state reaction from  $\text{CaO}$ ,  $\text{IrO}_2$ , and  $\text{PtO}_2$  powders. Well-ground mixtures of the starting material in a stoichiometric molar ratio were placed into an Au capsule ( $\phi = 2.5\text{ mm}$ ) sandwiched by BN composite disks ( $\phi = 2.7\text{ mm}$ ).  $\text{CaIr}_{0.5}\text{Rh}_{0.5}\text{O}_3$  was synthesized by solid-state reaction from  $\text{CaO}$ ,  $\text{IrO}_2$ , and  $\text{Rh}_2\text{O}_3$ , with  $\text{KClO}_4$  as an oxidizer. A well-ground mixture of the starting materials at a ratio of  $1/0.5/0.5/4.07$  ( $\text{Ca}/\text{Ir}/\text{Rh}/\text{O}$ ) was placed into an Au capsule ( $\phi = 2.5\text{ mm}$ ) sandwiched by  $\text{MgO}$  disks ( $\phi = 2.7\text{ mm}$ ), to avoid reducing conditions within the cell. The capsules were heated in a multi-anvil apparatus at  $1300^\circ\text{C}$  and  $15\text{GPa}$  pressure for 40 min, followed by rapid quenching to ambient temperature, and then release of pressure. Considerably high-pressure ( $15\text{GPa}$ ) was needed since the reduction of  $\text{PtO}_2$  followed by the phase separation of solid solutions (for example, the  $\text{Ir}/\text{Pt}$  ratio varied from 0.4 to 0.6 for  $\text{CaIr}_{0.5}\text{Pt}_{0.5}\text{O}_3$ ) was detected by SEM/EDX and a large amount of  $\text{IrO}_2$  impurity was detected by XRD when synthesis pressures were at  $\sim 3\text{ GPa}$  and  $\sim 10\text{GPa}$ . Extremely high-pressure ( $15\text{GPa}$ ) was needed in order to maximize the high oxygen pressure within the capsule in case of  $\text{CaIr}_{0.5}\text{Rh}_{0.5}\text{O}_3$ . Dense black pellets were obtained and that of  $\text{CaIr}_{0.5}\text{Rh}_{0.5}\text{O}_3$  was washed with distilled water to remove  $\text{KCl}$ .

High pressure Raman spectroscopy studies on  $\text{CaIr}_{0.5}\text{Pt}_{0.5}\text{O}_3$  were conducted using a laser-heated diamond anvil cell with  $\text{NaCl}$  pressure medium and Renishaw RS-SYS 1000 (Ar laser:  $\lambda = 514.5\text{ nm}$ ) at GRC. The sample was heated to  $\sim 1900\text{ K}$  for more than 10 minutes by using double-sided laser heating system ( $\lambda = 1072\text{ nm}$ ) installed at GRC. Pressures were estimated from diamond Raman shift<sup>13</sup>, and temperatures were determined by spectroradiometric measurements of the light emitted from the sample under heating. Ambient condition Raman

spectra on  $\text{CaIr}_{1-x}\text{Pt}_x\text{O}_3$  ( $x = 0.3, 0.5, 0.7$ ) and  $\text{CaIr}_{0.5}\text{Rh}_{0.5}\text{O}_3$  were collected using Lab-Raman (HeNe laser:  $\lambda = 632.8$  nm) at CSEC.

### III. Results and Discussion

Post-perovskite and perovskite type polymorphs of  $\text{CaMO}_3$  ( $M = \text{Ir/Pt}$ ) can be identified and distinguished at high pressure from their Raman spectra. Fig. 3 shows representative spectra of the polycrystalline  $\text{CaIrO}_3$  post-perovskite and  $\text{CaIr}_{0.7}\text{Pt}_{0.3}\text{O}_3$  post-perovskites and for the perovskite phase of polycrystalline  $\text{CaIrO}_3$  prepared at  $930^\circ\text{C}$  in an evacuated silica tube, which is noisier as this phase is metallic<sup>14</sup>. The post-perovskite phases are characterised by five prominent Raman modes, the frequencies of which are shown in Table 2. All of the modes harden at similar rates with pressure, as shown in the plot in Fig. 4. The asymmetry and the broadening of the Raman mode peaks observed for  $\text{CaIr}_{1-x}\text{Pt}_x\text{O}_3$  series ( $x = 0, 0.3, 0.5, 0.7$ ) and  $\text{CaIr}_{0.5}\text{Rh}_{0.5}\text{O}_3$  imply the beginning of the photo-induced metallization of these compounds since they only have a small band gap<sup>15</sup>.

The post-perovskite to perovskite structural transformation at the mid-point of the  $\text{CaIrO}_3$ - $\text{CaPtO}_3$  solid solution was explored through a high pressure Raman spectroscopy study.  $\text{CaIr}_{0.5}\text{Pt}_{0.5}\text{O}_3$  retains the post-perovskite structure on compression to 60 GPa in a DAC (diamond anvil cell) and the changes of Raman frequencies of shown in Table 2. Fig. 2 shows the room temperature Raman spectra of the sample at 60 GPa before and after laser-heating to  $\sim 1900$  K, and at several pressures during subsequent decompression to ambient pressure. Before heating the sample up to  $\sim 1900$  K, heating at lower temperatures ( $\sim 1500$  K and  $\sim 1700$  K) were tried, but their Raman spectra showed no indication of phase transition. Comparison with the spectra in Fig. 2, and that of  $\text{CaHfO}_3$  perovskite,<sup>16</sup> shows that  $\text{CaIr}_{0.5}\text{Pt}_{0.5}\text{O}_3$  transforms from post-perovskite ( $\text{CaIrO}_3$ ) type to perovskite type on heating at 60 GPa. The perovskite phase persists on decompression to 20 GPa, but reverts to the post-perovskite structure between 20 and 9 GPa. The Raman modes of the perovskite phase of  $\text{CaIr}_{0.5}\text{Pt}_{0.5}\text{O}_3$  are shown in Table 3 and are plotted against pressure in Fig. 5.

As the perovskite phase of  $\text{CaIr}_{0.5}\text{Pt}_{0.5}\text{O}_3$  transformed back into post-perovskite at  $\sim 9$  GPa, we conclude that Pt-doped  $\text{CaIrO}_3$  favours the post-perovskite structure over the perovskite structure at moderate pressures.

High pressure Raman spectroscopy studies on  $\text{CaIr}_{0.5}\text{Pt}_{0.5}\text{O}_3$  revealed that the five prominent Raman modes for post-perovskite phase show positive pressure dependence: 1.6 to 4.3 ( $\text{cm}^{-1}/\text{GPa}$ ) (Fig.4, Table 2). According to the group theory, there are 12 Raman-active modes

( $4A_g + 3B_{1g} + B_{2g} + 4B_{3g}$ ) out of 30 phonon modes ( $4A_g + 2A_u + 3B_{1g} + 6B_{1u} + B_{2g} + 6B_{2u} + 4B_{3g} + 4B_{3u}$ ) for *Cmcm* symmetry in post-perovskite regime. Thus, 5 out of 12 Raman-active modes were observed for each of the pressures in our study. The number of modes and their frequency are similar to the previously reported  $\text{CaIrO}_3$  high-pressure Raman spectra<sup>10</sup>, apart from the newly observed Raman mode near  $700\text{cm}^{-1}$ , which was in fact detectable in our study for  $\text{CaIr}_{1-x}\text{Pt}_x\text{O}_3$  series ( $x = 0, 0.3, 0.5, 0.7$ ) and  $\text{CaIr}_{0.5}\text{Rh}_{0.5}\text{O}_3$  by adopting the appropriate orientation of grains. The Ir and Pt atoms do not participate in the Raman-active phonon modes due to its atomic site symmetry (: 4a), while post-perovskite structure has 4 structural degree of freedom out of 12 atomic coordinates. As a reference, the Ir atoms in  $\text{CaIrO}_3$  post-perovskite and  $\text{CaIrO}_3$  perovskite do not participate in the Raman-active phonon modes either.

High pressure Raman spectroscopy studies on  $\text{CaIr}_{0.5}\text{Pt}_{0.5}\text{O}_3$  revealed that the seven prominent Raman modes for perovskite phase show positive pressure dependence:  $1.0$  to  $2.8$  ( $\text{cm}^{-1}/\text{GPa}$ ) (Fig.5, Table 3). However, the fifth Raman mode ( $\nu_5$ ) of the perovskite phase does not follow this trend. The anomalous pressure dependence of this Raman mode around  $28$  GPa implies a possible second-order phase transition. It is worthwhile to note that when the Raman modes of the perovskite phase of  $\text{CaIr}_{0.5}\text{Pt}_{0.5}\text{O}_3$  are extrapolated to ambient pressure, they have the same number of Raman modes below  $400\text{cm}^{-1}$  and similar mode frequencies with  $\text{CaMnO}_3$  perovskite<sup>17</sup> in *Pbnm* space group. This is reasonable since  $\text{CaIrO}_3$  perovskite is also in the space group of *Pbnm*. Therefore, the perovskite phase of  $\text{CaIr}_{0.5}\text{Pt}_{0.5}\text{O}_3$  is likely to be in the orthorhombic regime with  $\text{GdFeO}_3$ -type structure (space group: *Pbnm*) having its octahedron less distorted and tilted compared to that of  $\text{CaIrO}_3$  perovskite, since the presence of  $\text{Pt}^{4+}$  suppresses Jahn-Teller effect of  $\text{Ir}^{4+}$  in orthorhombic perovskite.

As the values of bulk modulus at ambient pressure for the post-perovskite phase of  $\text{CaIrO}_3$ <sup>18</sup> ( $K_0$ :  $180.2(28)$  GPa) and  $\text{CaPtO}_3$ <sup>11</sup> ( $K_0$ :  $174.0(5)$  GPa) calculated by in-situ X-ray diffraction studies are close to each other, it is a good estimation to assume that the bulk modulus of the post-perovskite phase of  $\text{CaIr}_{0.5}\text{Pt}_{0.5}\text{O}_3$  has the average value of these two values,  $K_0$ :  $177.1$  GPa. As the mode Grüneisen parameters ( $\gamma_{i,0}$ ) of each Raman mode is defined in the equation as follow, where  $\gamma_{i,0}$  is the mode Grüneisen parameter,  $K_{T0}$  is the bulk modulus at ambient temperature and  $\nu_{i,0}$  is the wavenumber of the  $\nu_i$  Raman mode at ambient pressure:

$$\gamma_{i,0} = K_{T0}/\nu_{i,0} * (d\nu_i / dP)$$

Table 2 shows the mode Grüneisen parameters ( $\gamma_{i,0}$ ) of the post-perovskite phase of  $\text{CaIr}_{0.5}\text{Pt}_{0.5}\text{O}_3$ , which can be calculated using the estimated bulk modulus at ambient conditions. The mode Grüneisen parameters ( $\gamma_{i,0}$ ) varied from 0.869 to 1.10 and  $\langle \gamma_{i,0} \rangle$  is 0.971 (Table 2), showing similar values and isotropy with those of  $\text{MgGeO}_3$ <sup>19</sup> instead of those of  $\text{CaIrO}_3$ <sup>10</sup>.  $\text{CaIr}_{0.5}\text{Pt}_{0.5}\text{O}_3$  has much smaller and much more isotropic mode Grüneisen parameters compared with  $\text{CaIrO}_3$ <sup>10</sup>. It is well known<sup>20</sup> that the weighted average of mode Grüneisen parameters by the Einstein heat capacity is in good match with the thermodynamic Grüneisen parameter  $\gamma_{\text{th}}$  (this is also the case for  $\text{CaIrO}_3$  post-perovskite). The weighted average of mode Grüneisen parameters  $[\gamma_{i,0}]$  for  $\text{CaIr}_{0.5}\text{Pt}_{0.5}\text{O}_3$  post-perovskite is 0.952 (Table 2), which is much smaller than the case of  $\text{CaIrO}_3$  post-perovskite ( $[\gamma_{i,0}]$ : 1.66). Thus, the weight average of mode Grüneisen parameters implies that  $\gamma_{\text{th}} \sim 0.952$  for  $\text{CaIr}_{0.5}\text{Pt}_{0.5}\text{O}_3$  post-perovskite. Such results suggest that  $\text{CaIr}_{0.5}\text{Pt}_{0.5}\text{O}_3$  is a better analogue of the post-perovskite phase of  $\text{MgSiO}_3$  than  $\text{CaIrO}_3$  as the triply degenerate ground state of low spin  $5d^5 \text{Ir}^{4+}$  is replaced by non-degenerate  $5d^6 \text{Pt}^{4+}$ . In addition, its estimated bulk modulus  $K_0$ : 177.1 GPa has similar a value with that of  $\text{MgSiO}_3$ <sup>21</sup> ( $K_0$ : 231 GPa) and  $\text{MgGeO}_3$ <sup>22</sup> ( $K_0$ : 205 GPa).

As the thermodynamic Grüneisen parameter  $\gamma_{\text{th}}$  can be calculated as:

$$\gamma_{\text{th}} = \alpha K_{\text{T}0} V / C_V \quad (\alpha: \text{thermal expansion parameter, } V: \text{cell volume, } C_V: \text{heat capacity})$$

, the thermal expansion and the heat capacity of  $\text{CaIr}_{0.5}\text{Pt}_{0.5}\text{O}_3$  post-perovskite will be very different from those of  $\text{CaIrO}_3$  post-perovskite due to the large gap in  $\gamma_{\text{th}}$ . The parameter  $q$ , which is the logarithmic volume derivative of Grüneisen parameters was also calculated for  $\text{CaIr}_{0.5}\text{Pt}_{0.5}\text{O}_3$  in order to compare it with that of  $\text{CaIrO}_3$ <sup>10</sup> and  $\text{MgGeO}_3$ <sup>18</sup>. The parameter  $q$  varied from 2.86 to 3.93, showing similar values with those of  $\text{MgGeO}_3$ <sup>18</sup> perovskite. It is worthwhile to note that unlike the case of the mode Grüneisen parameters, the parameter  $q$  has similar values with that of  $\text{CaIrO}_3$ <sup>10</sup>, especially for  $v_3$ .

As the experimentally derived bulk modulus at ambient pressure for perovskite phase of  $\text{CaIrO}_3$  is  $K_0$ : 198(3) GPa, which is not so far away from the bulk modulus of the post-perovskite phase of  $\text{CaIrO}_3$  either, it is constructive to assume that the extrapolated ambient pressure bulk modulus of the perovskite phase of  $\text{CaIr}_{0.5}\text{Pt}_{0.5}\text{O}_3$  is  $\sim 200$  GPa. Then, the mode Grüneisen parameters ( $\gamma_{i,0}$ ) of the perovskite phase of  $\text{CaIr}_{0.5}\text{Pt}_{0.5}\text{O}_3$  can be calculated as shown in Table 3.

The mode Grüneisen parameters ( $\gamma_{i,0}$ ) varied from 0.912 to 1.96 and the simple average  $\langle\gamma_{i,0}\rangle$  is 1.29, showing similar values and isotropy with those of  $\text{MgGeO}_3$ <sup>18</sup> perovskite. As the weighted average of mode Grüneisen parameters is  $[\gamma_{i,0}]$ : 1.27, we estimate that  $\gamma_{\text{th}} \sim 1.27$  for  $\text{CaIr}_{0.5}\text{Pt}_{0.5}\text{O}_3$  perovskite. Therefore, the thermodynamic Grüneisen parameter increases by 33 % across the post-perovskite to perovskite phase transition in  $\text{CaIr}_{0.5}\text{Pt}_{0.5}\text{O}_3$ . A similar magnitude of increase in  $\gamma_{\text{th}}$  is reported for  $(\text{Mg,Fe})\text{SiO}_3$ <sup>23</sup> (27 %) and  $\text{MgGeO}_3$ <sup>18</sup> (33 %). In addition, the perovskite phase of  $\text{CaIr}_{0.5}\text{Pt}_{0.5}\text{O}_3$  has the same number of prominent Raman modes as  $\text{MgGeO}_3$ <sup>18</sup> perovskite. Therefore,  $\text{CaIr}_{0.5}\text{Pt}_{0.5}\text{O}_3$  is a promising analogue of  $\text{MgSiO}_3$  system in the lowermost mantle. The parameter  $q$  was not calculated since the pressure dependence of Raman modes of the perovskite phase of  $\text{CaIr}_{0.5}\text{Pt}_{0.5}\text{O}_3$  were close to linear, having similar feature with the  $\text{MgGeO}_3$ <sup>18</sup> perovskite. It would be useful to conduct  $\text{CaIrO}_3$  perovskite high-pressure Raman studies for comparison, but this is extremely difficult since the Raman peaks are very noisy due to its metallic<sup>14</sup> feature.

The Raman mode near  $563 \text{ cm}^{-1}$ , which is present for  $\text{CaIr}_{1-x}\text{Pt}_x\text{O}_3$  ( $x = 0.3, 0.5, 0.7$ ) and not visible for  $\text{CaIrO}_3$ , indicates that the strong attraction of O atoms toward the Pt atoms plays an important role in the vibration regarding  $\text{PtO}_6$  octahedron. In other words, the strengthening of the vibration modes that are responsible for O atoms due to the slightly stronger attraction of O atoms toward the Pt atoms gives rise to the Raman mode near  $563 \text{ cm}^{-1}$ .

#### IV. Discussion

The newly synthesized phase at 60GPa, ~1900K for  $\text{CaIr}_{0.5}\text{Pt}_{0.5}\text{O}_3$  has Raman modes which resemble those of  $\text{CaIrO}_3$  perovskite and  $\text{CaHfO}_3$  perovskite, suggesting this phase has a perovskite structure. However, this perovskite phase transformed back into a post-perovskite phase when the pressure was released down to ~9GPa. According to the previous studies on phase transition from post-perovskite to perovskite in  $\text{CaIrO}_3$ <sup>8</sup>, the phase equilibrium boundary is calculated to be  $P \text{ (GPa)} = 0.040 T \text{ (K)} - 67.1$ . Thus, the phase equilibrium boundary condition for  $\text{CaIrO}_3$  at  $T = 1900\text{K}$  is predicted to be  $P = 8.9\text{GPa}$  from the strongly positive  $P/T$  slope. Therefore, assuming the gradient of the  $P/T$  slope is uniform over the  $\text{CaIr}_{1-x}\text{Pt}_x\text{O}_3$  series, the theoretical phase boundary between post-perovskite and perovskite phase for  $\text{CaPtO}_3$  is estimated as ~111GPa for ~1900K and ~87GPa for ~1300K by extrapolating the  $P/T$  phase boundary for  $\text{CaIrO}_3$  (8.9GPa, 1900K) and  $\text{CaIr}_{0.5}\text{Pt}_{0.5}\text{O}_3$  (60GPa, 1900K). Taking such estimations into



consideration, the observation that  $\text{CaPtO}_3$ <sup>9</sup> did not transform into perovskite phase at 7GPa and ~1300K suggests the lack of synthesis pressure for a perovskite phase. Thus, even though the phase transition from post-perovskite to perovskite may take place at extremely high pressures (above 80GPa), it is likely that the perovskite phase reverts back to post-perovskite structure at lower pressures. In other words, the instability of the perovskite phase of  $\text{CaPtO}_3$  has been revealed by the destabilization of newly synthesized perovskite phase of  $\text{CaIr}_{0.5}\text{Pt}_{0.5}\text{O}_3$ .

The conflict between the strong Pt-O covalent bonding that favours large octahedral tilting and the Jahn-Teller inactive  $\text{Pt}^{4+}$  in perovskite regime which favour cubic perovskite is one possible reason for destabilization of the perovskite-structure. A similar destabilization mechanism of perovskite- against ilmenite-structure has been previously explained in the case of  $\text{NaSbO}_3$ -type oxides<sup>24</sup>. In conclusion, the conflict between the strong Pt-O covalent bonding that favours large octahedral tilting and the Jahn-Teller inactive  $\text{Pt}^{4+}$  in perovskite structure which favour cubic regime is one possible reason for destabilization of the perovskite-structure, while pressure and the replacement of Pt-O by Ir-O bonding can play a role in sustaining perovskite structure. In the case of  $\text{CaIrO}_3$ ,  $\text{CaRhO}_3$  and  $\text{CaRuO}_3$ , this conflict does not exist since the B-site cation ( $\text{Ir}^{4+}$ :  $5d^5$ ,  $\text{Rh}^{4+}$ :  $4d^5$ ,  $\text{Ru}^{4+}$ :  $4d^4$ ) in each compound is Jahn-Teller active. In other words, the instability of the perovskite phase of  $\text{CaIr}_{0.5}\text{Pt}_{0.5}\text{O}_3$  has revealed why post-perovskite to perovskite phase transition has not been observed for  $\text{CaPtO}_3$  unlike the case for  $\text{CaIrO}_3$ ,  $\text{CaRhO}_3$  and  $\text{CaRuO}_3$ . The stability condition of post-perovskite/perovskite regime is very sensitive since  $\text{Ir}^{4+}$  and  $\text{Pt}^{4+}$  in  $\text{CaMO}_3$  ( $\text{M} = \text{Ir/Pt}$ ) have similar ionic radii ( $\text{Ir}^{4+}$ : 0.625,  $\text{Pt}^{4+}$ : 0.625) and similar electronegativity ( $\chi_{\text{Ir}}$ : 2.2,  $\chi_{\text{Pt}}$ : 2.28). The strong Pt-O covalent bonding that stabilizes post-perovskite regime comes from the high electronegativity of Pt. The post-perovskite phase of  $\text{CaIrO}_3$ ,  $\text{CaPtO}_3$ ,  $\text{CaRhO}_3$  and  $\text{CaRuO}_3$  can be quenched to ambient pressure since the electronegativity of Ir, Pt, Rh and Ru are 2.20, 2.28, 2.28 and 2.20, while that of Si, Ge, Al, Fe and Mn are 1.90, 2.01, 1.61, 1.83 and 1.55, respectively. Therefore,  $\text{MgSiO}_3$ <sup>19</sup>,  $\text{MgGeO}_3$ <sup>20</sup>,  $\text{Al}_2\text{O}_3$ <sup>25</sup>,  $\text{Fe}_2\text{O}_3$ <sup>2</sup> and  $\text{Mn}_2\text{O}_3$ <sup>3</sup> can take the post-perovskite structure at high pressures, but when the compression of bonds due to high confining pressure is removed, the strong M-O covalent bonding ( $\text{M} = \text{Si/Ge/Al/Fe/Mn}$ ) disappears and it can no longer sustain the post-perovskite structure. It has been reported that  $\text{Al}^{3+}$  incorporation<sup>26</sup> in the Si-site of the post-perovskite phase of  $\text{MgSiO}_3$  is much more difficult than in the Si-site of  $\text{MgSiO}_3$  perovskite and requires stabilization pressure higher than 130GPa. This is in good agreement with the fact that Si has higher electronegativity than Al. In other words, the incorporation of  $\text{Al}^{3+}$  in the Si-site will stabilize the perovskite-regime and destabilize the post-perovskite regime. Si has higher electronegativity than any existing elements of  $\text{M}^{3+}$  or  $\text{M}^{4+}$  ( $\text{M} = \text{Al, Fe, Ti, Mn, Zr}$ ) in the

lowermost mantle. Therefore, substitutions of the Si-site by M (M = Al, Fe, Ti, Mn, Zr) will be destabilized at lowermost mantle conditions and can only be stabilized by pressures higher than in the lowermost mantle. Thus, the high electronegativity which plays a key role in the stability of post-perovskite phase of  $\text{CaIr}_{0.5}\text{Pt}_{0.5}\text{O}_3$  leads to an important implication: the Si-site of the post-perovskite phase of  $\text{MgSiO}_3$  is free from any substitution in the lowermost mantle.

## V. Conclusions

The new phase synthesized at 60GPa, 1900K for  $\text{CaIr}_{0.5}\text{Pt}_{0.5}\text{O}_3$  has Raman modes which resemble those of  $\text{CaIrO}_3$  perovskite, suggesting this phase has a perovskite structure. Pt-O covalent bonding due to the high electronegativity of Pt stabilizes the post-perovskite structure and destabilizes the perovskite structure, while pressure and the replacement Pt-O by Ir-O bonding can play a role in sustaining the perovskite structure. The instability of the perovskite phase of  $\text{CaIr}_{0.5}\text{Pt}_{0.5}\text{O}_3$  reveals why the post-perovskite to perovskite phase transition has not been observed for  $\text{CaPtO}_3$  unlike the case for  $\text{CaIrO}_3$ ,  $\text{CaRhO}_3$  and  $\text{CaRuO}_3$ . Furthermore, we predict that the Si-site of the post-perovskite phase of  $\text{MgSiO}_3$  is free from any substitution in the lowermost mantle. High pressure Raman spectroscopy studies on  $\text{CaIr}_{0.5}\text{Pt}_{0.5}\text{O}_3$  reveal that the five primary Raman modes for post-perovskite phase and seven primary Raman modes for perovskite phase show positive pressure dependence: 1.6 to 4.3 ( $\text{cm}^{-1}/\text{GPa}$ ) for post-perovskite phase and 1.0 to 2.8 ( $\text{cm}^{-1}/\text{GPa}$ ) for perovskite phase. We estimated the increase in  $\gamma_{\text{th}}$  across the post-perovskite to perovskite transition, which is in similar magnitude with  $(\text{Mg,Fe})\text{SiO}_3$  and  $\text{MgGeO}_3$ , suggesting that  $\text{CaIr}_{0.5}\text{Pt}_{0.5}\text{O}_3$  is a promising analogue for investigating  $\text{MgSiO}_3$  system in the lowermost mantle.

Table 1: The five primary Raman modes of  $\text{CaIr}_{1-x}\text{Pt}_x\text{O}_3$  and  $\text{CaIr}_{0.5}\text{Rh}_{0.5}\text{O}_3$

Wavenumber ( $\text{cm}^{-1}$ )	$\text{CaIrO}_3$	$\text{CaIr}_{0.7}\text{Pt}_{0.3}\text{O}_3$	$\text{CaIr}_{0.5}\text{Pt}_{0.5}\text{O}_3$	$\text{CaIr}_{0.3}\text{Pt}_{0.7}\text{O}_3$	$\text{CaIr}_{0.5}\text{Rh}_{0.5}\text{O}_3$
$\nu_1$	309	322	320	334	301
$\nu_2$	444	452	451	452	449
$\nu_3$	552	543	544	553	546
$\nu_4$	-----	562	559	568	565
$\nu_5$	712	688	692	703	648

Table 2: The five primary Raman modes of post-perovskite phase of  $\text{CaIr}_{0.5}\text{Pt}_{0.5}\text{O}_3$  at high pressures along with the mode Grüneisen parameters ( $\gamma_{i,0}$ ) and its logarithmic volume derivative  $q$

P (GPa)	$\nu_1(\text{cm}^{-1})$	$\nu_2(\text{cm}^{-1})$	$\nu_3(\text{cm}^{-1})$	$\nu_4(\text{cm}^{-1})$	$\nu_5(\text{cm}^{-1})$
0	322	448	545	565	692
9	337	467	586	599	733
30	378	534	651	681	840
50	403	569	693	748	917
60	416	582	714	766	943
$\gamma_{i,0}$	0.869	0.913	0.894	1.08	1.10
$q$	2.86	3.84	3.93	2.93	3.11

Simple average of  $\gamma_{i,0}$ ,  $\langle \gamma_{i,0} \rangle$  : 0.971

Weighted average of  $\gamma_{i,0}$ ,  $[\gamma_{i,0}]$  : 0.952

Table 3: The seven primary Raman modes of perovskite phase of  $\text{CaIr}_{0.5}\text{Pt}_{0.5}\text{O}_3$  at high pressures along with the mode Grüneisen parameters ( $\gamma_{i,0}$ )

P (GPa)	$\nu_1(\text{cm}^{-1})$	$\nu_2(\text{cm}^{-1})$	$\nu_3(\text{cm}^{-1})$	$\nu_4(\text{cm}^{-1})$	$\nu_5(\text{cm}^{-1})$	$\nu_6(\text{cm}^{-1})$	$\nu_7(\text{cm}^{-1})$
20	164	181	208	263	295	314	377
28	178	193	233	268	282	340	389
38	190	203	258	282	306	364	408
60	206	223	292	312	349	426	445
$\gamma_{i,0}$	1.23	1.13	1.96	0.966	1.05	1.76	0.912

Simple average of  $\gamma_{i,0}$ ,  $\langle \gamma_{i,0} \rangle$  : 1.29

Weighted average of  $\gamma_{i,0}$ ,  $[\gamma_{i,0}]$  : 1.27

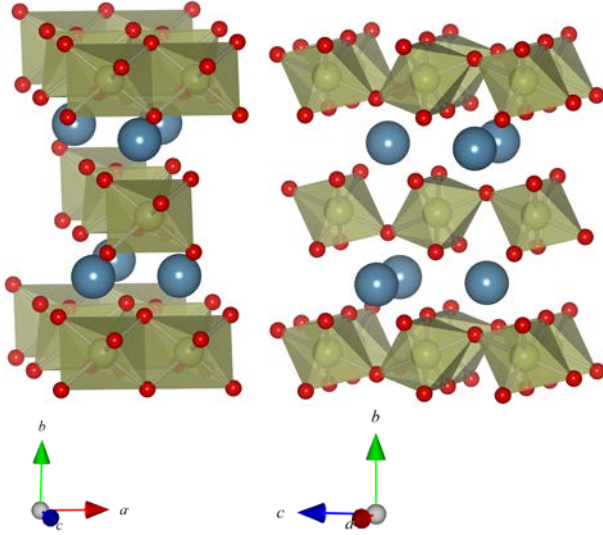


Fig.1: Crystal structure of  $\text{CaIrO}_3$  in edge-sharing and corner-sharing projection

Fig.2: Raman spectra of  $\text{CaIr}_{0.5}\text{Pt}_{0.5}\text{O}_3$  at high pressure conditions for (a) 60GPa, RT before heating the sample by laser, (b) 60GPa, RT after heating the sample upto 1900K by laser, (c) pressure released down to 38GPa after laser heating, (d) pressure released down to 20GPa after laser heating, (e) pressure released down to 9GPa after laser heating

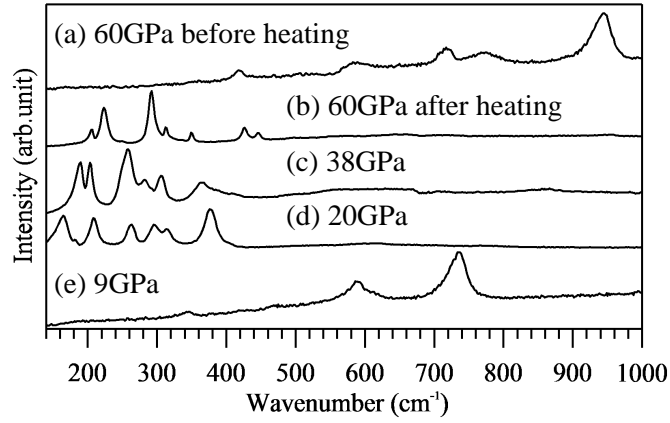


Fig.3: Raman spectra of (a)  $\text{CaIrO}_3$  perovskite, (b)  $\text{CaIrO}_3$  post-perovskite and (c)  $\text{CaIr}_{0.7}\text{Pt}_{0.3}\text{O}_3$

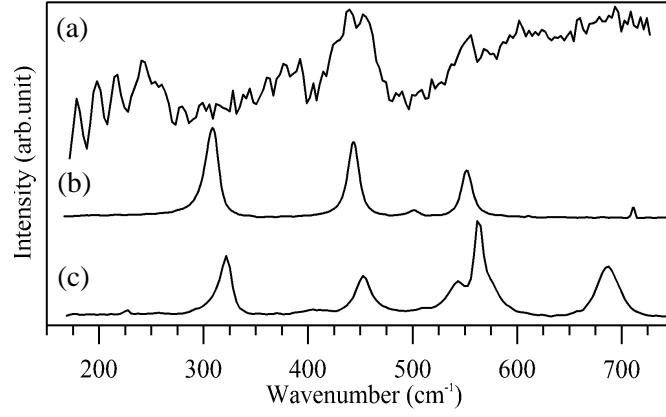


Fig.4: Pressure dependence of the five primary Raman modes of  $\text{CaIr}_{0.5}\text{Pt}_{0.5}\text{O}_3$  post-perovskite (  $\nu_1$ : n ,  $\nu_2$ : l ,  $\nu_3$ : s ,  $\nu_4$ : t ,  $\nu_5$ :  $\Lambda$  )

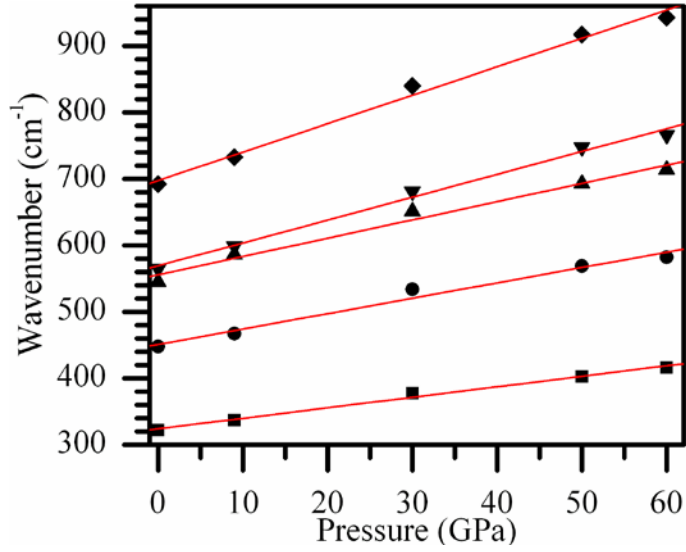
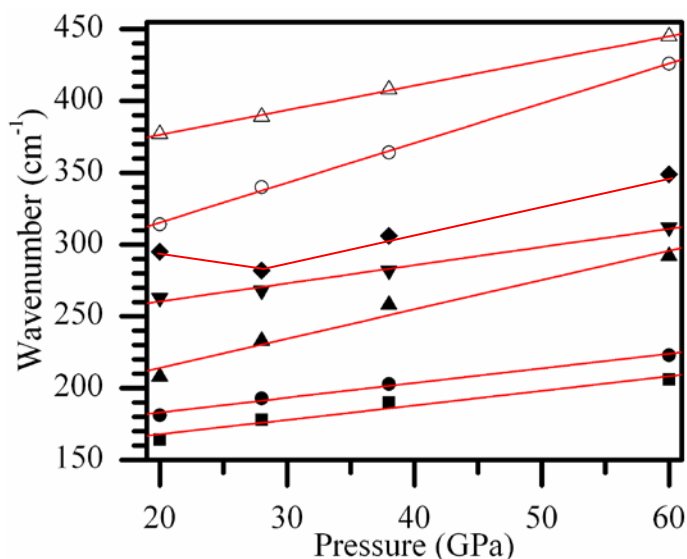


Fig.5: Pressure dependence of the seven primary Raman modes of  $\text{CaIr}_{0.5}\text{Pt}_{0.5}\text{O}_3$  perovskite (  $\nu_1$ : n ,  $\nu_2$ : l ,  $\nu_3$ : s ,  $\nu_4$ : t ,  $\nu_5$ :  $\Lambda$  ,  $\nu_6$ : m ,  $\nu_7$ : 8 )



## References:

- <sup>1</sup> Murakami, M; Hirose, K; Kawamura, K; Sata, K; Ohishi, Y *Science*, 2004, 304, 855-858
- <sup>2</sup> Shim, S; Bengtson, A; Morgan, D; Sturhahn, W; Catalli, K; Zhao, J; Lerche, M; Prakapenka, V.B. *PNAS*, **2009**, 106, 5508-5512
- <sup>3</sup> Santillán, J; Shim, S; Shen, G; Prakapenka, V.B. *Geophys. Res. Lett.*, **2006**, 33, L15307
- <sup>4</sup> Hirai, S; Welch, M.D; Aguado, F; Redfern, S.A.T *Z. Kristallogr.*, **2009**, 224, 345-350
- <sup>5</sup> Ohgushi, K; Matsushita, Y; Miyajima, N; Katsuya, Y; Tanaka, M; Izumi, F; Gotou, H; Ueda, Y; Yagi, T *Physics and Chemistry of Minerals*, **2008**, 35, 189-195
- <sup>6</sup> Yamaura, K; Shirako, Y; Kojitani, H; Arai, M; Young, D.P.; Akaogi, M; Nakashima, M; Katsumata, T; Inaguma, Y; Takayama-Muromachi, E *J. Am. Chem. Soc.*, **2009**, 131, 2722-2726
- <sup>7</sup> Kojitani, H; Shirako, Y; Akaogi, M *Physics of the Earth and Planetary Interiors*, **2007**, 165, 127-134
- <sup>8</sup> Kojitani, H; Furukawa, A; Akaogi, M *Am. Mineral.*, **2007**, 92, 229-232
- <sup>9</sup> Inaguma, Y; Hasumi, K; Yoshida, M; Ohba, T; Katsumata, T *Inorg. Chem.*, **2008**, 47, 1868-1870
- <sup>10</sup> Hustoft, J; Shim, S; Kubo, A; Nishiyama, N *Am. Mineral.*, **2008**, 93, 1654-1658
- <sup>11</sup> Lindsay-Scott, A; Wood, I.G.; Dobson D.P.; Vočadlo, L; Brodholt, J.P.; Crichton, W; Hanfland, M; Taniguchi, T *Physics of the Earth and Planetary Interiors*, **2010** to be published
- <sup>12</sup> Ohgushi, K; Gotou, H; Yagi, T; Kiuchi, Y; Sakai, F; Ueda, Y *Phys. Rev. B*, **2006**, 74, 241104
- <sup>13</sup> Akahama, Y; Kawamura, H *J. Appl. Phys.*, **2004**, 96, 3748-3751
- <sup>14</sup> Sarkozy, R.F.; Moeller, C.W.; Chamberland, B.L. *J. Solid State Chem.*, **1974**, 9, 242-246
- <sup>15</sup> Hirai, S; Sanehira, T; Nishiyama, N; Irifune, T; Klemme, S; Bromiley, G; Attfield, J.P. *Chem. Mater.* to be published
- <sup>16</sup> Park, C.I.; Condrate, R.A.; Snyder, R. L. *Appl. Spectr.*, **1976**, 30, 352-353
- <sup>17</sup> Abrashev, M.V.; Bäckström, J; Börjesson, L; Popov, V.N.; Chakalov, R.A.; Kolev, N; Meng, R.L.; Iliev, M.N. *Phys. Rev. B*, **2002**, 65, 184301
- <sup>18</sup> Martin, C.D.; Chapman, K.W.; Chupas, P.J.; Prakapenka, V; Lee, P.L.; Shastri, S.D.; Parise, J.B. *Am. Mineral.*, **2007**, 92, 1048-1053
- <sup>19</sup> Shim, S; Kubo, A; Duffy, T.S. *Earth and Planet. Sci Lett.*, **2007**, 260, 166-178
- <sup>20</sup> Chopelas, A; Boehler, R.; Ko, T. *Physics and Chemistry of Minerals*, **1994**, 21, 351-359.

- 
- <sup>21</sup> Tuchiya, T; Tuchiya, J; Umemoto, K; Wentzcovitch, R.M. *Geophys. Res. Lett.*, **2004**, *31*, L14603
- <sup>22</sup> Kubo, A; Kiefer, B; Shim, S; Shen, G; Prakapenka, V.B. ; Duffy, T.S *Am. Mineral.*, **2008**, *93*, 965-976
- <sup>23</sup> Shim, S; Catalli, K; Hustoft, J; Kubo, A; Prakapenka, V.B.; Caldwell, W.A.; Kunz, M *PNAS*, **2008**, *105*, 7382–7386
- <sup>24</sup> Mizoguchi, H; Woodward, P.M.; Byeon, S; Parise, J.B. *J. Am. Chem. Soc.*, **2004**, *126*, 3175-3184
- <sup>25</sup> Oganov, A.R.; Ono, S *PNAS*, **2005**, *102*, 10828-10831
- <sup>26</sup> Zhang, F; Oganov, A.R. *Earth and Planet. Sci Lett.*, **2006**, *248*, 54-61